Fabrication of size-tunable hierarchical CrN nanohole arrays for two-dimensional nanomould using modified nanosphere lithography

Hung-Chun Wu[1,2], *MingDong Bao*[1], *Kung-Jeng Ma*[2]

[1]*School of Materials Science and Engineering, Ningbo University of Technology, Ningbo 315016, People's Republic of China*
[2]*College of Engineering, Chung Hua University, Hsin Chu 300, Taiwan*
E-mail: hungchunwu@gmail.com

Published in Micro & Nano Letters; Received on 4th February 2014; Revised on 18th May 2014; Accepted on 17th June 2014

This Letter presents a low-cost, high-throughput strategy for fabricating size-tunable hierarchical CrN nanohole arrays for a nanomould using a magnetron sputtering approach with nanosphere lithography (NIL)-based technology. The size of the polystyrene nanospheres has a direct influence on the diameter and period of the CrN nanohole structure. The reactive ion etching and magnetron sputtering process can easily control the nanohole size and depth. The hole depth generally depends on the film thickness. The contact angles were measured by the sessile drop method using distilled water, ethylene glycol and diiodomethane. The surface-free energy of the CrN nanomould was calculated using the Owens–Wendt geometric mean approach. This Letter reports the successful fabrication of a series of nanoholes with diameters decreased from 347 ± 9.6 to approximately 166 ± 11.8 nm with a depth of 100 ± 5.6 nm. The corresponding surface-free energy decreased from 40.83 to approximately 24.58 mN/m. The diameter of nanoholes has an obvious effect on the surface-free energy and there is tendency for the surface-free energy to decrease with the decrease in the diameter of the nanoholes. This new approach of ordered CrN nanohole array structures can be used to create a two-dimensional nanomould for NIL.

1. Introduction: Periodic nanostructure arrays have received widespread attention in recent years because of their unique properties and potential applications in optoelectronics [1], photonic crystals [2], catalysis [3] and so on. Several techniques are capable of fabricating the periodic arrays of nanostructure, including electrochemical etching [4], X-ray lithography methods [5], electron-beam lithography (EBL) [6] and molecular-beam epitaxy (MBE) [7]. Although lithographic techniques can control the morphology of these arrays, their high-cost and sophisticated processes limit their practicality. Therefore, numerous researchers have attempted to develop low-cost, high-throughput and high-resolution lithography techniques. One alternative approach, called the nanoimprint lithography (NIL) technique [8] has the potential of producing large-scale nanostructures and can replicate nanopatterns numerous times. However, numerous technical challenges remain to be solved in the development of NIL, including the problem of nanomould preparation and the anti-sticking effect (high contact angle and low surface-free energy). The development of new low surface-free energy coating materials has become critical to improving performance. The low surface-free energy of the proposed nanomould structure requires a closed-field unbalanced magnetron sputtering ion plating system to deposit the thin film of CrN. This approach has been widely used to prepare hard ceramic coatings with excellent friction, thermal stability, anti-sticking and corrosion resistance properties [9, 10]. The nanosphere lithography (NSL) technique has the advantages of being low-cost and simple. This technique is also a high-throughput method that is attractive for the fabrication of the ordered CrN nanohole arrays in a nanomould [11, 12]. This Letter reports the fabrication of a large-scale, ordered, two-dimensional (2D) nanomould with low surface-free energy and periodic nanoholes for NIL using modified NSL. This study also investigates the surface-free energy effect of the CrN nanohole structure using a contact angle experiment.

2. Experimental: Polystyrene (PS) nanospheres with a mean diameter of 540 nm were purchased from Bangs Laboratories Inc. as 10wt% in colloidal aqueous suspensions. Fig. 1 shows a detailed procedure for fabricating a nanomould of large-scale periodic CrN nanohole arrays using NSL. First, the Si(100) wafer was diced into 15×15 mm pieces. To create a hydrophilic surface, the silicon substrates were ultrasonically cleaned by submerging them into a 1:1 mixture of aqueous ammonia (NH_4OH) and hydrogen peroxide (H_2O_2) solution for 30 minutes, and then washed with deionised (DI) water for 10 minutes. The periodic arrays of the PS nanosphere monolayer templates were created by a self-assembly process using a spin coater at a speed of 1200 rpm for 4 minutes, and the size of the nanospheres was controlled by reactive ion etching (RIE) processing using oxygen as the etching gas. After controlling the size of the PS nanospheres, the CrN nanomould structures were deposited on Si (100) substrates using a closed-field unbalanced magnetron sputtering ion plating system (CFUBMIP, Huijin Teer Coatings Ltd, UDP650) with chromium targets. Nitrogen flow was automatically controlled using a closed-loop optical emission monitor control unit. From the unbalanced magnetron sputtering plasma, Cr^{+2} emission intensity was set at a wavelength of 425 nm [13]. A fibre optic cable then directed the Cr^{+2} emission from the plasma zone to the OEM control unit's photomultiplier. A comparison is given by the UBM reading which shows the relative intensity of Cr^{+2} emissions compared with the 100% emission intensity at the metal sputtering mode [13]. After the sputtering chamber was pumped to a base pressure of 1.5×10^{-5} torr, a mass flow controller introduced high-purity argon gas into the chamber at a flow rate of 25 sccm. The bias voltage was set at -70 V with a Cr target current for 1 A. A CrN nanomould coating measuring 100 nm thick was deposited at an OEM setting of 60%. An explanation of the formation of a nanohole, this is expected considering the formation of a nanohole due to use of the directional sputtering allows the CrN to fill in the interstices of the PS nanospheres directly. Hence, no or little under-deposition around the bottom of the colloid nanospheres would be expected. Recently some reports in the literature are focused on the development of nanodot or nanohole arrays using the PVD process while using NSL [14, 15]. Therefore the CrN nanohole structure arrays were formed using the directional sputtering process while using the NSL-based technology. After deposition of the CrN thin film, an ultrasonic wash in dichloromethane

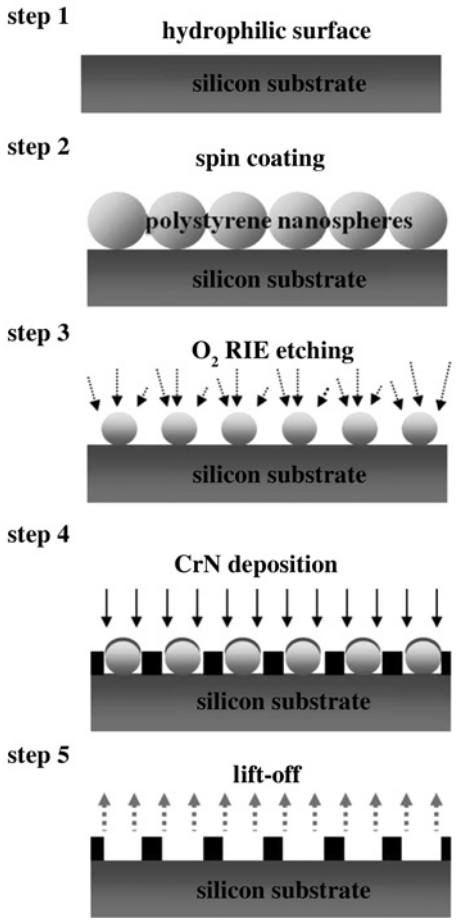

Figure 1 *Schematic diagrams of the fabrication procedures for a nanomould with an ordered CrN nanohole array structure using nanosphere lithography*

(CH_2Cl_2) for 10 minutes removed the template. CH_2Cl_2 dissolved and lifted off the PS nanospheres. Finally, the samples were ultrasonically cleaned in acetone (CH_3COCH_3) and then in ethanol (C_2H_5OH) for 5 minutes. The resulting CrN nanohole array nanomould had a well-ordered 2D periodic structure.

Nanostructure and preferred orientation of nanomoulds were analysed by X-ray diffraction (XRD; Cu Ka1 irradiation). The surface and cross-sectional morphology of the ordered CrN nanohole arrays of nanomoulds were observed using a scanning electron microscope (SEM; Hitachi S-4800 Cold Field Emission). The topography of the ordered CrN nanohole arrays of nanomoulds were measured by using an atomic force microscope (AFM; NanoScope III System Digital Instrument) in the tapping mode. The contact angles were measured by a contact angle system (Dataphysics OCA-20 contact angle analyser) with using the sessile drop method. The digital drop image was used as an image analysis system and calculated both the left and right contact angles from the shape of the drop with an accuracy of ±0.1°. Three test liquids were measured by using as a probe for the surface-free energy calculations: distilled water (θW), ethylene glycol (θE) and diiodomethane (θD). The contact angle values were obtained by averages of three measurements made on different areas of the sample surface.

3. Results and discussion: This Letter reports the successful fabrication of PS nanospheres in a large-area monolayer hexagonally close-packed arrangement on a Si substrate using a spin-coating method (Figs. 2*a* and *c*). After the closed-packed monolayer was formed, an O_2 RIE process with an RF power of 50 W for 20 minutes further reduced the size of the PS nanosphere

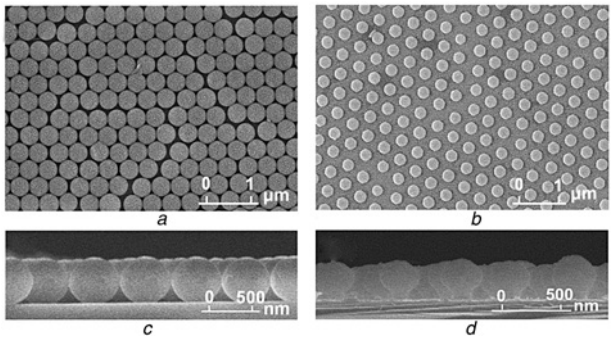

Figure 2 *SEM images for various size of nanosphere arrays*
a Top view and
c Cross-sectional view of the spin coated monolayer PS nanosphere arrays with 540 nm diameter on a clean glass substrate
b Top view and
d Cross-sectional view of the PS nanosphere colloidal ion etched by O_2 RIE at 50 W for 20 min

mask (Figs. 2*b* and *d*). The high-quality long-range periodic monolayer of the PS nanosphere arrays can be maintained after the O_2 RIE process. The nanosphere diameter changed from 540 nm to approximately 290 ± 5.4 nm.

The colloidal monolayer templates produced a large-scale 2D ordered of size-varied 540 nm periodic CrN nanohole array (Fig. 3). The inset in Fig. 3*a* shows high magnification of cross-sectional view by 90° tilting the CrN nanohole. The ordered CrN nanohole array structure has a circular shape from the top view,

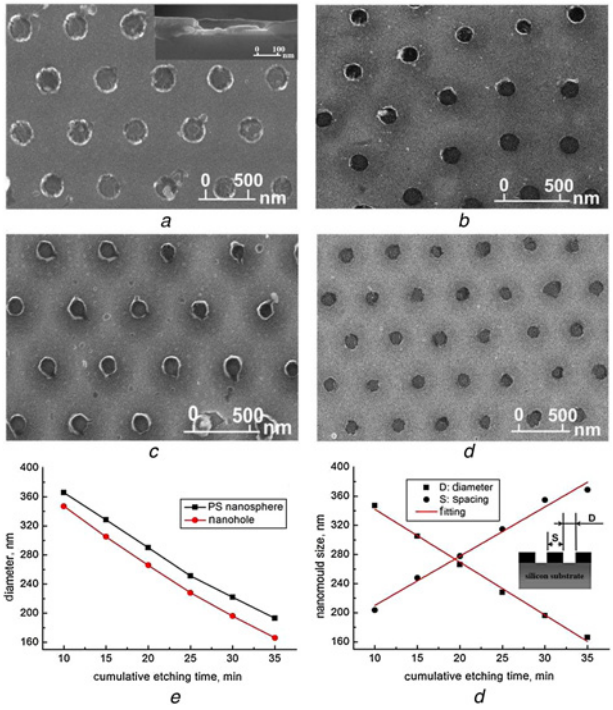

Figure 3 *SEM images of sizes-varied ordered CrN nanohole arrays of nanomould*
Images (a), (b), (c) and (d) were obtained by the colloidal templates and thinned by RIE process with 50 W for 10, 20, 25 and 35 min, respectively
The inset shows (a) the high magnification of cross-sectional view by 90° tilting the CrN nanohole
The sizes-varied ordered CrN nanohole arrays statistics of nanomould
Image (e) shows the diameter of PS nanosphere and nanohole statistics of a series of samples
Image (f) shows the etching time dependency of diameter and spacing between two nanohole structures with 540 nm in period

doi: 10.1049/mnl.2014.0013

and the surface morphology exhibits a nanohierarchical structure. These ordered CrN nanohole array films are considerably rougher than the relative flat surface, and exhibit certain protuberances on the nanohole walls of a large nanohole (Fig. 3*a*).

The diameter of the nanoholes was smaller than the PS nanospheres (Fig. 3*e*), which the mean value of difference is about 25 nm. The high-quality long-range periodic monolayer of the PS nanosphere arrays can be maintained after the O_2 RIE process. The diameter of nanosphere changed from 376 ± 5.3 nm to approximately 190 ± 3.4 nm. The diameter of the CrN nanomould with nanohole decreased from 347 ± 9.6, 266 ± 11.3, 228 ± 11.6 to approximately 166 ± 11.8 nm, respectively. Thus, this produced CrN nanomoulds with highly ordered nanohole structures and large areas. The construction of a linear relationship between the diameter and the spacing of the nanoholes and the RIE etching time can be used to control the dimensional accuracy of the nanoholes and the pattern of the array (Fig. 3*f*). Hence, this approach changes the diameter of the nanohole without changing the centre-to-centre (CTC) spacing between two adjacent holes.

The distribution of diameter of CrN nanoholes varies were obtained by the colloidal templates and thinned by RIE process, and then deposited on Si(100) substrates using magnetron sputtering process, as shown in Figs. 4*a–f*. The standard deviation ΔL, the mean value of diameter $\langle L \rangle$ and the dispersion $\delta = \Delta L / \langle L \rangle$ are obtained. All of the data from every nanohole can be fitted by a Gaussian function and the fitting curves are also given using a red curve in every plot. Summary of the mean values of diameter for the ordered CrN nanohole array of the nanomould is plotted in Fig. 4*g*. The dispersion of diameter for every CrN nanohole is plotted in Fig. 4*h*. It can be seen that the O_2 RIE etching time is increased from 10 to 35 minutes, and the corresponding the dispersion of diameter increases from 2.8% to approximately 7.1%. However, the value of δ influenced by O_2 RIE process is only about 1.6% [16]. Therefore this can be attributed to the diameter dispersion mainly caused by the deposition process of CrN thin film and then lift-off of PS nanosphere process has slight influences. This is because of the PS nanosphere size decreases, deposition process of CrN thin film on the surface of the nanosphere relative increase thus leading to increased difficulty lift-off process. The linear relationship between the mean of diameter and etching time will help to control the final dimensional accuracy of nanohole prepared using RIE etching approach.

Fig. 5*a* shows the AFM images and depth profiles of the CrN nanohole array nanomould fabricated by colloidal templates using O_2 RIE at 50 W for 10 minutes on Si substrates, followed by CrN deposition and then lift-off PS nanosphere processes. Image (a) shows the side view and a corresponding line scan of the 2D topography surface and depth profiles, indicating that the nanohole depth was approximately 100 ± 5.6 nm. Image (b) shows the XRD measurements of the CrN nanohole structure grown on Si(100) substrates in the range of 10–90 (2θ). The XRD pattern of the CrN nanohole indicates three peaks which preferred orientations are indexed to (111) and (200) plane. The CrN films were indexed to a NaCl-type structure. CrN (200) has the lowest surface-free energy and (111) the lowest strain energy [17].

This study shows the measurement of the contact angles of the three test liquids on the CrN ordered nanohole arrays of the nanomould surface. When the contact angles decreased, the nanohole diameter increased (Fig. 6*a*). The dependence curve between the nanohole diameter and contact angles showed significant variations in the contact angle values on the ordered CrN nanohole array structure. For the surface roughness, Wenzel presented a model describing the water dewetting behaviour of nanohole films; the following equation is obtained [18]

$$\cos \theta r = r \cos \theta \tag{1}$$

where r is the roughness factor, and θr and θ are the contact angles on the nanohole film and native film, respectively. According to Wenzel's equation, high roughness can enhance both the hydrophobicity of the hydrophobic surface and the hydrophilicity of the hydrophilic surface.

Based on the morphology and topography of the nanomould of the ordered CrN nanohole array structure, these ordered CrN

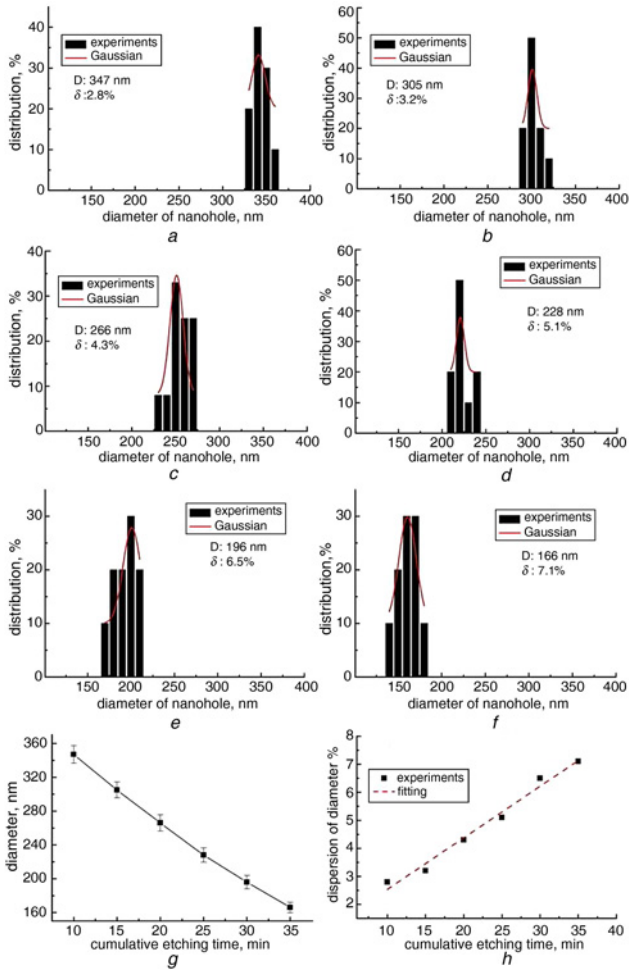

Figure 4 *Histograms show diameter distribution of CrN nanohole of nanomoulds using the colloidal templates and thinned by RIE process with 50 W for a 10 minutes b 15 minutes c 20 minutes d 25 minutes e 30 minutes and f 35 minutes, respectively g Summary of the mean values of diameter h Relationship between dispersion of diameter and RIE etching time*

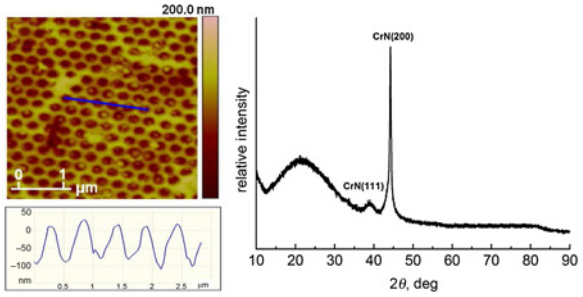

Figure 5 *a AFM 2D topography surface of the nanomould of ordered CrN nanohole arrays which were fabricated by colloidal templates using the RIE process with O_2 plasma of 50 W for 10 min on Si substrates, followed by CrN deposition and lift-off PS nanosphere processes b XRD spectrum of the ordered CrN nanohole arrayed structures fabricated by using a closed field unbalanced magnetron sputtering ion plating system*

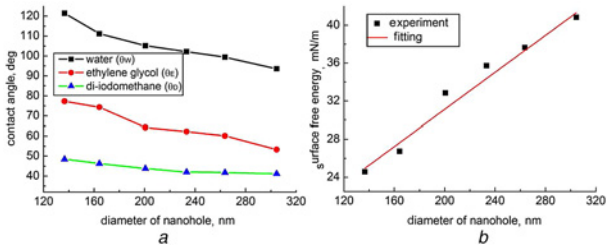

Figure 6 *Relationships to the nanohole diameter*
a Relationship between the nanohole diameter and the contact angles of three test liquids
b Relationship between the nanohole diameter and the surface-free energy

nanohole array films are substantially rougher than the relatively flat surface. The roughness of ordered CrN nanohole array films increased as the nanohole size increased due to the numerous protuberances on the nanohole walls. Thus, the Wenzel model can explain why the nanohole array films exhibit hydrophilicity, and why this hydrophilicity increased as the nanohole size increased. Conversely, this indicates that the roughness of the ordered CrN nanohole array films decreased as the nanohole size decreased, producing certain protuberances on the nanohole walls of a large nanohole size. Equation (1) shows that θr should increase, which agrees with the current results in Figs. 3*a*–*c*.

This study investigates the surface-free energy rather than the contact angle, and therefore presents the results in terms of the surface-free energy. In general, the CrN coatings with a larger contact angle value imply lower surface-free energy. Therefore, the CrN coatings have a good anti-adhesive effect, and can be applied to moulding components [9]. Three test liquids were used as a probe for the surface-free energy calculations at a surface temperature of 20°C.

The surface tension of distilled water at 20°C was calculated using data from Vargaftik *et al.* [19]: $\gamma_L = 72.8$ mN/m, $\gamma_L^d = 21.8$ mN/m and $\gamma_L^P = 51.0$ mN/m. The surface tension of distilled water was estimated by using the following equation

$$\gamma_L = 235.8\left(\frac{374 - T}{647.15}\right)^{1.256}\left[1 - 0.625\left(\frac{374 - T}{647.15}\right)\right] \quad (2)$$

where T (°C) is the distilled water temperature.

The surface tension of ethylene glycol at 20°C was obtained using the data from Jho and Carreras [20]: $\gamma_L = 48.0$ mN/m, $\gamma_L^d = 29.0$ mN/m and $\gamma_L^p = 19.0$ mN/m. The surface tension of ethylene glycol was estimated by using the following equation

$$\gamma_L = 46.97 - \frac{T}{15} \quad (3)$$

where T (°C) is the ethylene glycol temperature.

The surface tension of diiodomethane at 20°C was obtained using the data from Zhao *et al.* [21]: $\gamma_L = 50.8$ mN/m, $\gamma_L^d = 50.8$ mN/m and $\gamma_L^p = 0$ mN/m. The surface tension of diiodomethane was estimated using the following equation

$$\gamma_L = 53.48 - 0.1415T + 4.9567 \times 10^{-5}T^2 \quad (4)$$

where T (°C) is the diiodomethane temperature. According to the above three empirical equations, the contact angle of at least two liquids with known surface tension components (γ_L, γ_L^d and γ_L^P) on the solid must be determined. The data for the test liquid surface tension and surface tension components at a surface temperature of 20°C were obtained using these three empirical equations. The solid surface-free energy can be calculated by measuring the fluid contact angle. This measurement method is based on Young's equation, which is expressed in a balanced formula of solid–liquid interface as follows [22]

$$\gamma_L \cos\theta = \gamma_S - \gamma_{SL} \quad (5)$$

where γ_L is the experimentally determined surface tension of the liquid, θ is the contact angle, γ_S is the surface-free energy of the solid and γ_{SL} is the solid–liquid interfacial energy. However, an estimate of γ_{SL} must be obtained to obtain solid surface-free energy γ_S. The contact angle values of the surface-free energy of the samples were calculated using the Owens–Wendt geometric mean approach [23]. This approach extends the Fowkes equation by including the hydrogen bonding term, and uses a geometric mean to combine the dispersion force and hydrogen bonding components giving the following equation

$$\gamma_{SL} = \gamma_S + \gamma_L - 2\sqrt{\gamma_S^d \gamma_L^d} - 2\sqrt{\gamma_S^p \gamma_L^p} \quad (6)$$

From the Young (5), it follows that

$$\gamma_L = (1 + \cos\theta) = 2\sqrt{\gamma_S^d \gamma_L^d} + 2\sqrt{\gamma_S^p \gamma_L^p} \quad (7)$$

To obtain the γ_S^d and γ_S^p values of a thin film, the contact angle of at least two liquids with known surface tension components (γ_L, γ_L^d and γ_L^p) on the solid must be determined. The surface-free energy was calculated using the contact angle test at 20°C on the nanomould surface of the ordered CrN nanohole arrays.

Fig. 6*b* shows the relationship between the nanohole diameter and the surface-free energy. The surface-free energy increases linearly as the nanohole diameter increases because the contact angle can enhance the decrease in nanohole roughness. Thus, the water contact angle increases as the nanohole diameter decreases (Fig. 6*a*), which implies a lower surface-free energy. Through the introduction of the CFUBMIP system sputtering deposition process, the ordered CrN nanohole structure surface has low surface energy at the interface. This can eliminate the sticking problem regarding the nanomould surface during demoulding. Therefore a low surface-free energy in the nanomould is required to meet the ever-increasing demands of NIL. The diameter of nanohole decreases from 305 ± 7.5 to approximately 136 ± 4 nm and the surface-free energy decreases from 40.83 to approximately 24.58 mN/m. The ordered CrN nanohole structure obtained the lowest surface-free energy. Therefore, this shows the fabrication of a 2D nanomould of low surface-free energy, large-scale, well-ordered, periodic nanoholes for NIL using modified NSL. The nanomould surface when the diameter of nanohole decreased with decreasing the surface-free energy. The ordered CrN nanohole array of the nanomould has an anti-sticking property that can be applied in the problems of the friction and sticking during demoulding. This new approach of fabricating an ordered CrN nanohole structure can be used to form a 2D nanomould for NIL.

4. Conclusion: In conclusion, this Letter reports a low-cost and high-throughput strategy for fabricating size-tunable hierarchical CrN nanohole arrays nanomould using modified NSL. The RIE and CrN coating process can easily control the periodicity and density of CrN hole-shaped nanostructure arrays with a controlled diameter and inter-particle spacing. The diameter of nanoholes has an obvious effect on the surface-free energy and there is tendency for the surface-free energy to decrease with decreasing nanoholes with diameters. The data on the surface-free energy of CrN nanomould at different diameter of nanoholes will contribute to demoulding design and operation for NIL.

5. Acknowledgments: This work was supported by the Zhejiang Provincial Natural Science Foundation (No. Y4100385) and Hi-Tech research and development program of Ningbo (Nos. 2009B10010 and 2007A22001).

doi: 10.1049/mnl.2014.0013

6 References

[1] Dang X.D., Tamayo A.B., Seo J., Hoven C.V., Walker B., Nguyen T.Q.: 'Nanostructure and optoelectronic characterization of small molecule bulk heterojunction solar cells by photoconductive atomic force microscopy', *Adv. Funct. Mater.*, 2010, **20**, pp. 14–21

[2] Chang Y.-C., Wu H.-W., Chen H.-L., Wang W.-Y., Chen L.-J.: 'Two-dimensional inverse opal ZnO nanorod networks with photonic band gap', *J. Phys. Chem. C*, 2009, **113**, pp. 14778–14782

[3] Schwenzer B., Gomm J.R., Morse D.E.: 'Substrate-induced growth of nanostructured zinc oxide films at room temperature using concepts of biomimetic catalysis', *Langmuir*, 2006, **22**, pp. 9829–9831

[4] Sun L., Chien C.-L.: 'Searson PC. Fabrication of nanoporous nickel by electrochemical dealloying', *Chem. mater.*, 2004, **16**, pp. 3125–3129

[5] Zhao X.-M., Xia Y., Whitesides G.M.: 'Soft lithographic methods for nano-fabrication', *J. Mater. Chem.*, 1997, **7**, pp. 1069–1074

[6] Fujita J., Ohnishi Y., Ochiai Y., Matsui S.: 'Ultrahigh resolution of calixarene negative resist in electron beam lithography', *Appl. Phys. Lett.*, 1996, **68**, pp. 1297–1299

[7] Jeong S.Y., Kim J.Y., Yang H.D., *ET AL.*: 'Synthesis of silicon nanotubes on porous alumina using molecular beam epitaxy', *Adv. Mater.*, 2003, **15**, pp. 1172–1176.

[8] Chou S.Y., Krauss P.R., Renstrom P.J.: 'Imprint of sub-25 nm vias and trenches in polymers', *Appl. Phys. Lett.*, 1995, **67**, p. 3114

[9] Wang D.-Y., Chiu M.-C.: 'Characterization of Cr_2O_3 CrN duplex coatings for injection molding applications', *Surf. Coat. Technol.*, 2001, **137**, pp. 164–169

[10] Han S., Chen H.-Y., Chang K.-L., *ET AL.*: 'Effects of MEVVA-implanted chromium on the structure and properties of CrN film', *Thin Solid Films*, 2004, **447**, pp. 425–429

[11] Wu H.-C., Chien H.-H., Ma K.-J., Bao M.-D.: 'Fabrication of size-tunable Cr nanodots and nanorings array by modified nanosphere lithography', *Micro Nano Lett.*, 2012, **7**, pp. 1056–1059

[12] Chien H.-H., Wu H.-C.: 'Fabrication of size-tunable hierarchical porous Cr nanoring arrays by modified nanosphere lithography', *Micro Nano Lett.*, 2012, **7**, pp. 1033–1037

[13] Wang D.-Y., Lin J.-H., Ho W.-Y.: 'Study on chromium oxide synthesized by unbalanced magnetron sputtering', *Thin Solid Films*, 1998, **332**, pp. 295–299

[14] Klein M.J.K., Guillaumeel M., Wenger B., *ET AL.*: 'Inexpensive and fast wafer-scale fabrication of nanohole arrays in thin gold films for plasmonics', *Nanotechnology*, 2010, **21**, p. 205301

[15] Tan B.J.Y., Sow C.H., Koh T.S., Chin K.C., Wee A.T.S., Ong C.K.: 'Fabrication of size-tunable gold nanoparticles array with nanosphere lithography, reactive ion etching, and thermal annealing', *J. Phys. Chem. B*, 2005, **109**, pp. 11100–11109

[16] Wu H.-C., Chien H.-H., Ma K.-J., Bao M.-D., Ho Y.-H.: 'Fabrication of Cr nanoring arrays by nanosphere lithography for light extraction', *Optoelectron. Adv. Mater.*, 2012, **6**, pp. 1019–1025

[17] Gautier C., Machet J.: 'Study of the growth mechanisms of chromium nitride films deposited by vacuum ARC evaporation', *Thin Solid Films*, 1997, **295**, pp. 43–52

[18] Wenzel R.N.: 'Resistance of solid surfaces to wetting by water', *Ind. Eng. Chem.*, 1936, **28**, pp. 988–994

[19] Vargaftik N.B., Volkov B.N., Voljak L.D.: 'International tables of the surface tension of water', *J. Phys. Chem. Ref. Data*, 1983, **12**, p. 817

[20] Jho C., Carreras M.: 'The effect of viscosity on the drop weight technique for the measurement of dynamic surface tension', *J. Colloid Interf. Sci.*, 1984, **99**, pp. 543–548

[21] Zhao Q., Liu Y., Abel E.: 'Effect of temperature on the surface free energy of amorphous carbon films', *J. Colloid Interf. Sci.*, 2004, **280**, pp. 174–183

[22] Young T.: 'An essay on the cohesion of fluids', *Trans. R. Soc. London*, 1805, **95**, pp. 65–87

[23] Owens D.K., Wendt R.: 'Estimation of the surface free energy of polymers', *J. Appl. Polymer Sci.*, 1969, **13**, pp. 1741–1747